International Journal of Plasticity 28 (2012) 124–140

Contents lists available at ScienceDirect

International Journal of Plasticity

journal homepage: www.elsevier.com/locate/ijplas

Multiscale modeling of plasticity based on embedding the viscoplastic self-consistent formulation in implicit finite elements

Javier Segurado [a], Ricardo A. Lebensohn [b,*], Javier LLorca [a], Carlos N. Tomé [b]

[a] Madrid Institute for Advanced Studies of Materials (IMDEA Materials Institute), Department of Materials Science, Polytechnic University of Madrid, C/Profesor Aranguren s/n, 28040 Madrid, Spain
[b] Materials Science and Technology Division, Los Alamos National Laboratory, MS G755, Los Alamos, NM 87845, USA

ARTICLE INFO

Article history:
Received 5 April 2011
Received in final revised form 11 July 2011
Available online 22 July 2011

Keywords:
B. Polycrystalline material
B. Anisotropic material
B. Crystal plasticity
A. Microstructures
C. Finite elements

ABSTRACT

This paper is concerned with the multiscale simulation of plastic deformation of metallic specimens using physically-based models that take into account their polycrystalline microstructure and the directionality of deformation mechanisms acting at single-crystal level. A polycrystal model based on self-consistent homogenization of single-crystal viscoplastic behavior is used to provide a texture-sensitive constitutive response of each material point, within a boundary problem solved with finite elements (FE) at the macroscale. The resulting constitutive behavior is that of an elasto-viscoplastic material, implemented in the implicit FE code ABAQUS. The widely-used viscoplastic selfconsistent (VPSC) formulation for polycrystal deformation has been implemented inside a user-defined material (UMAT) subroutine, providing the relationship between stress and plastic strain-rate response. Each integration point of the FE model is considered as a polycrystal with a given initial texture that evolves with deformation. The viscoplastic compliance tensor computed internally in the polycrystal model is in turn used for the minimization of a suitable-designed residual, as well as in the construction of the elasto-viscoplastic tangent stiffness matrix required by the implicit FE scheme.

Uniaxial tension and simple shear of an FCC polycrystal have been used to benchmark the accuracy of the proposed implicit scheme and the correct treatment of rotations for prediction of texture evolution. In addition, two applications are presented to illustrate the potential of the multiscale strategy: a simulation of rolling of an FCC plate, in which the model predicts the development of different textures through the thickness of the plate; and the deformation under 4-point bending of textured HCP bars, in which the model captures the dimensional changes associated with different orientations of the dominant texture component with respect to the bending plane.

1. Introduction

The formulation of multiscale frameworks for modeling and simulation of plastic deformation of polycrystalline materials is a very active field of research, representing at the same time a challenging material science and computational problem and a relevant development for engineering applications. The main goal is to simultaneously account for the strength of the actual deformation mechanisms active at single-crystal level, the polycrystalline character of the aggregate microstructure and its evolution with deformation, and the specific boundary conditions applied to a polycrystalline specimen.

* Corresponding author. Tel.: +1 505 665 3035; fax: +1 505 667 8021.
E-mail addresses: jsegurado@mater.upm.es (J. Segurado), lebenso@lanl.gov (R.A. Lebensohn), javier.llorca@imdea.org (J. LLorca), tome@lanl.gov (C.N. Tomé).

0749-6419/$ - see front matter © 2011 Elsevier Ltd. All rights reserved.
doi:10.1016/j.ijplas.2011.07.002

Since its inception by Peirce et al. (1982), the so-called *crystal plasticity finite element (CPFE)* method has been extensively used to solve problems involving the mechanical behavior of crystalline materials. This methodology combines (single) crystal plasticity (CP) as constitutive description and finite element (FE) analysis as numerical solver for boundary-value problems (for a comprehensive review of these methods, see e.g. Roters et al. (2010)). While most of the CPFE applications found in the literature are based on the numerical solution of single-crystal plasticity constitutive equations directly within the FE analysis (in most cases, with intragranular resolution, i.e. comprising several integration points and, usually, several elements per grain), the present approach can be regarded as belonging to a sub-class of models based on CP and FE, in which the single crystal (microscopic) behavior is connected with the specimen (macroscopic) response through an intermediate (mesoscopic) scale. The behavior at this latter scale is obtained from the homogenized response of an entire polycrystal, which represents the behavior of each material point in the FE mesh.

This kind of approach, based on polycrystal homogenization at the mesoscale, is applicable to problems with a clear *separation of scales*, i.e. those in which the typical length-scale associated with the gradients of the mechanical fields at the macroscale is large compared with the typical length-scale of the polycrystalline microstructure (e.g. the grain or sub-grain size).

Different flavors of models and numerical methods at both ends of this multiscale problem are well-established and readily available. In this work, the *microscopic scale* represented by single crystals deforming by slip and twinning, is modeled by means of the *rate-sensitivity approach* to plasticity (e.g. Asaro and Needleman, 1985) and a description of strain-hardening based on a phenomenological update of the critical resolved shear stresses of the different deformation modes (e.g. Tomé et al., 1984). This latter choice involves the identification of a relatively small number of constitutive parameters, although the modifications to the present implementation to include more sophisticated hardening laws, (e.g. Beyerlein and Tomé, 2007, 2008; Proust et al., 2007) are straight-forward. The *macroscopic scale*, represented by an elasto-viscoplastic solid, possibly of complicated geometry and undergoing complex boundary conditions, is modeled with the commercial FE code ABAQUS (2007), in its *implicit* version. This choice guaranties in principle a greater efficiency for the same accuracy, compared to explicit formulations, and a relatively easy portability of the present development, in the form of a user-defined material (UMAT) subroutine.

In what concerns the *mesoscopic scale*, the techniques used at this level can be of different kind. For example, they can be based on purely *numerical homogenization*, in which the micromechanical fields are fully resolved inside each polycrystalline unit cell associated with each macroscopic integration point, and averaged to obtain the material point's response. Within this group, FE has been frequently used to perform this mesoscale numerical homogenization for different polycrystalline microstructures (e.g. Miehe et al., 1999; Werwer and Cornec, 2000; Kouznetsova and Geers, 2008). In the general case of heterogeneous materials (of which a polycrystal is a particular case), these approaches are sometimes referred to as *FE^2 models* (e.g. Feyel, 2003). Alternatively, as in the present work, the mesoscopic homogenization can rely on more efficient *mean-field theories*, in which the polycrystal response is obtained from an estimate of its effective behavior, based on some overriding principle (e.g. iso-strain, iso-stress, energy minimization) and a statistical representation of the microstructure.

Another important aspect of the implementation of the mesoscopic level within the multiscale analysis concerns whether the polycrystal model is (Van Houtte et al., 2006): (a) *embedded* in the FE computation, i.e. interrogated on the fly each time the behavior of the corresponding material point is needed by the FE analysis, or (b) it is used in a *hierarchical* fashion, such that the FE level utilizes a number of parameters which are identified in advance (pre-computed), using the mesoscale model (Van Houtte et al., 2006, 2009). Embedded models are obviously more accurate to follow the microstructural evolution and how the latter affects the macroscopic behavior, while hierarchical approximations are more efficient. In connection with these two different strategies, it is also worth mentioning a promising intermediate approach, known as *adaptative sampling (AS)* method (Barton et al., 2008), which consists in embedding a lower length-scale model (e.g. at polycrystal level) and storing, each time this model is interrogated, the response obtained for a given microstructure. In this way, a microstructure-response database is populated, which can be used instead of a new call to the polycrystal model when the current microstructure is not far from an already computed point of this microstructure-response space.

In the present work, the strategy of fully embedding a mean-field model in the FE analysis is used at mesoscopic scale. In particular, we use polycrystal models based on self-consistent (SC) homogenization of single-crystal plastic behavior. This choice (under which the constituent single crystals deform differently according to their orientation and their interaction with the surrounding material), instead of the simpler Taylor iso-strain approximation (under which the strains of the crystals are assumed to be equal to the strain of the aggregate), provides in general a more accurate texture-sensitive constitutive response of the polycrystalline material points. In particular, we make use of the viscoplastic self-consistent (VPSC) approach. This formulation, based on a ad-hoc linearization of the non-linear single crystal constitutive behavior and the use of the linear SC model (Hershley, 1954), was first proposed by Molinari et al. (1987) for the prediction of texture evolution of polycrystalline materials, and later extended and numerically implemented by Lebensohn and Tomé (1993) in the so-called VPSC code. In the last decade, the VPSC formulation and code have experienced several improvements and extensions (e.g. see Lebensohn et al., 2007), and it is nowadays extensively used to simulate plastic deformation of polycrystalline aggregates (considered as single material points) and to interpret experimental evidence on metallic, geological and polymeric materials (see Lebensohn et al. (2007) for a comprehensive list of VPSC applications).

While this is not the first attempt to embed polycrystal models in FE codes to connect single crystal and macroscopic behaviors, novel relevant aspects of the present formulation will be described here and compared with earlier approaches. Mathur and Dawson (1989) used a rigid-viscoplastic Eulerian FE approach to model the evolution of crystallographic texture during a steady-state rolling process, obtaining the response of the polycrystalline aggregates associated with each material

point from an iso-strain Taylor assumption. Also based on a Taylor-type homogenization at the level of the polycrystalline material points, Kalidindi et al. (1992) developed an elasto-viscoplastic implementation in ABAQUS, using an implicit time-integration scheme for the simulation of texture evolution in non-steady forming operations. While the procedure reported in Kalidindi et al. (1992) for the calculation of the Jacobian matrix was based on numerical differentiation, later Kalidindi and collaborators (e.g. Delannay et al., 2006) implemented more efficient analytical schemes to obtain this Jacobian within a Taylor framework. Kalidindi (1998) was also the first to incorporate twinning at the mesoscale (using a Taylor framework) within ABAQUS.

In what concerns the use of mesoscopic viscoplastic self-consistent schemes in FE codes, the applications to date consisted in *explicit* implementations, for problems involving hcp materials in which plasticity at single-crystal level was accommodated not only by slip but also by twinning (see Tomé et al. (2001) and Kaschner et al. (2001) for Zr, using the FE code EPIC; and Walde and Riedel (2007a,b) for Mg, using ABAQUS explicit). The obvious motivation for these applications is the superior ability of the VPSC formulation (e.g. Lebensohn and Tomé, 1993; Tomé et al., 2001) compared with the Taylor model to capture the strong texture-induced anisotropy of hcp polycrystals, the rapid textural changes induced by twinning that results in strong geometric hardening/softening, as well as the highly anisotropic slip-twin interaction. In contrast with these previous VPSC-FE couplings, in the present implementation the self-consistent polycrystal model is embedded in an *implicit* FE code. In addition to the benefits of using an implicit formulation (robustness and less computational cost for the same accuracy), a key and novel aspect of this coupling is that the tangent stiffness matrix (Jacobian) of the non-linear FE scheme is obtained analytically, what makes the implementation less computationally expensive. This stiffness matrix is obtained as a function of the viscoplastic tangent moduli (which has already been calculated as part of the non-linear self-consistent homogenization scheme), the elastic stiffness of the aggregate, and the FE time increment.

2. Model

At the macroscopic scale, the proposed multiscale approach is a standard elasto-viscoplastic FE with implicit time integration, which solves the governing equations under certain imposed boundary conditions and given constitutive relations between strain increments and stresses at the level of the integration points. In order to obtain such constitutive behavior, a whole polycrystal is considered at each integration point. In turn, the mesoscopic VPSC model is interrogated to obtain the homogenized viscoplastic response of each of these *polycrystalline material points*, as needed during the FE solution of the macroscopic boundary problem. Upon convergence of the macroscopic model, the microstructure of each polycrystal is updated in terms of the average values of the micromechanical fields inside the crystallites, obtained through *localization* relations, which are natural by-products of the self-consistent solution.

2.1. Kinematics

The proposed UMAT with the VPSC solver at the mesoscale is devised to work under a small-strain approximation, and for finite deformations as well. Given that the VPSC formulation is rigid-viscoplastic, in the case of small strains, an additive decomposition of the total strain increment ($\Delta\boldsymbol{\varepsilon}$), in elastic ($\Delta\boldsymbol{\varepsilon}_{el}$) and viscoplastic ($\Delta\boldsymbol{\varepsilon}_{vp}$) parts is assumed, such that the constitutive relation at each polycrystalline integration point is given by:

$$\Delta\boldsymbol{\varepsilon} = \Delta\boldsymbol{\varepsilon}_{el} + \Delta\boldsymbol{\varepsilon}_{vp} = \boldsymbol{C}^{-1} : \Delta\boldsymbol{\sigma} + \Delta\boldsymbol{\varepsilon}_{vp} \tag{1}$$

where $\boldsymbol{C}$ is the elastic stiffness of the polycrystalline material point, $\Delta\boldsymbol{\sigma}$ is the Cauchy stress increment, and $\Delta\boldsymbol{\varepsilon}_{vp} = \Delta\boldsymbol{\varepsilon}_{vp}(\boldsymbol{\sigma})$ is computed with the VPSC model for each polycrystalline material point.

In the case of large deformations, our implementation is consistent with ABAQUS's default treatment of rotations. A *local coordinate system*, defined by the unit vectors $\mathbf{e}_\alpha$ ($\alpha = 1, 3$) in which the polycrystal behavior is computed, undergoes rotations that need to be accounted for by the FE. In what follows, this system will also be referred to as *co-rotational system*. In the present *hypoelastic* solution of the finite-deformation problem, the material model is formulated incrementally, using the Jaumann rate as the objective rate to define the stress increments (although other choices are possible, e.g. Peeters et al. (2001)). In this case, the evolution of the unit vectors of the local coordinate system rotating with the polycrystal is given by:

$$\dot{\mathbf{e}}_\alpha = \dot{\boldsymbol{\omega}} \cdot \mathbf{e}_\alpha \tag{2}$$

where $\dot{\boldsymbol{\omega}}$ is the total rotation-rate of the polycrystalline material point. The integration of $\dot{\boldsymbol{\omega}}$ in a time increment (from time t to $t + \Delta t$) gives an incremental rotation matrix $\Delta\mathbf{R}$ that rotates the local reference system from time t to $t + \Delta t$:

$$\mathbf{R}^{t+\Delta t} = \Delta\mathbf{R} \cdot \mathbf{R}^t \tag{3}$$

where $\mathbf{R}^{t+\Delta t}$ is the rotation matrix from the local coordinate system at $t = 0$ to its orientation at time $t + \Delta t$,[1] e.g.

$$\mathbf{e}_\alpha^{t+\Delta t} = \mathbf{R}^{t+\Delta t} \cdot \mathbf{e}_\alpha^0 \tag{4}$$

[1] Note that, in general, the rotation matrix calculated incrementally can be different from the one defined by the polar decomposition of the deformation gradient $\mathbf{F}$ ($\mathbf{F} = \mathbf{R} \cdot \mathbf{U}$).

Similarly to Eq. (1), for large strains the velocity-gradient $\mathbf{L}$ is decomposed into elastic and viscoplastic components:

$$\mathbf{L} = \mathbf{L}_{el} + \mathbf{L}_{vp} \tag{5}$$

where:

$$\mathbf{L}_{el} = \dot{\boldsymbol{\varepsilon}}_{el} + \dot{\boldsymbol{\omega}} \tag{6a}$$

$$\mathbf{L}_{vp} = \dot{\boldsymbol{\varepsilon}}_{vp} \tag{6b}$$

Elastic and viscoplastic constitutive laws involve only the symmetric component of the deformation, while the antisymmetric component is ambiguous. Consequently, for convenience, in Eq. (6) the full rotation-rate was assigned to the elastic part of the velocity-gradient, although other choices can be made (e.g. Barton et al., 2008).

The Jaumann rate of the Kirchoff stress, which is the stress measure work-conjugate with the rate of deformation, is defined by:

$$\overset{\triangledown}{\boldsymbol{\tau}} = \dot{\boldsymbol{\sigma}} - \dot{\boldsymbol{\omega}} \cdot \boldsymbol{\sigma} + \boldsymbol{\sigma} \cdot \dot{\boldsymbol{\omega}} \tag{7}$$

If plastic strains are much larger than elastic ones, deformation can be considered isochoric ($J = \det(\mathbf{F}) = 1$ and $\boldsymbol{\tau} = J\boldsymbol{\sigma} \approx \boldsymbol{\sigma}$). Thus, $\overset{\triangledown}{\boldsymbol{\sigma}}$ is related to the elastic strain-rate by:

$$\overset{\triangledown}{\boldsymbol{\sigma}} = \boldsymbol{C} : (\dot{\boldsymbol{\varepsilon}} - \dot{\boldsymbol{\varepsilon}}_{vp}) \tag{8}$$

The FE solution requires constitutive relation (8) be expressed and integrated in a fixed coordinate system. Let us assume that the coordinate system associated to every polycrystalline material point at $t = 0$ is unique and given by $\mathbf{e}^0_\alpha$, and let us use this reference frame as the required fixed coordinate system. Integrating Eq. (8) from time t to $t + \Delta t$ gives:

$$\overset{\triangledown}{\boldsymbol{\sigma}}\,\Delta t = \boldsymbol{C} : (\Delta\boldsymbol{\varepsilon} - \Delta\boldsymbol{\varepsilon}_{vp}) \tag{9}$$

In our formulation, the polycrystal elastic stiffness and the viscoplastic strain increment are calculated by means of the VPSC model in the co-rotational system. Therefore, in order for these magnitudes to be expressed in the fixed coordinate system, use is made of $\mathbf{R}^{t+\Delta t}$, e.g. if $\Delta\boldsymbol{\varepsilon}^*_{vp}$ is the viscoplastic strain increment computed by means of the VPSC model (the symbol "$*$" denotes magnitudes expressed in the co-rotational system), $\Delta\boldsymbol{\varepsilon}_{vp}$ to be used in Eq. (9) is obtained as:

$$\Delta\boldsymbol{\varepsilon}_{vp} = (\mathbf{R}^{t+\Delta t})^T \cdot \Delta\boldsymbol{\varepsilon}^*_{vp} \cdot \mathbf{R}^{t+\Delta t} \tag{10}$$

In Eq. (9), $\Delta\boldsymbol{\varepsilon}$ is the logarithmic strain increment, obtained from $\Delta\boldsymbol{\varepsilon}^*$ given by the FE analysis:

$$\Delta\boldsymbol{\varepsilon}^* = \log(\Delta\mathbf{V}) \tag{11}$$

with $\Delta\mathbf{V}$ being the left Cauchy stretch tensor associated with the deformation gradient increment from time t to $t + \Delta t$, such that: $\Delta\mathbf{F} = \Delta\mathbf{V} \cdot \Delta\mathbf{R}$. Hence:

$$\Delta\boldsymbol{\varepsilon} = (\mathbf{R}^{t+\Delta t})^T \cdot \Delta\boldsymbol{\varepsilon}^* \cdot \mathbf{R}^{t+\Delta t} \tag{12}$$

Finally, for completeness, once the right-hand of Eq. (9) is obtained by computing the left-hand magnitudes in the fixed reference system, the stress expressed in co-rotational axes (as needed by VPSC as part of the proposed algorithm, see next section) is obtained as:

$$\boldsymbol{\sigma}^{t+\Delta t^*} = \mathbf{R}^{t+\Delta t} \cdot (\boldsymbol{\sigma}^t + \overset{\triangledown}{\boldsymbol{\sigma}}\,\Delta t) \cdot (\mathbf{R}^{t+\Delta t})^T \tag{13}$$

2.2. Viscoplastic single-crystal and polycrystal models

At polycrystal level, the use of a rigid-viscoplastic approach implies that the constitutive relations at single-crystal level can be expressed in terms of Cauchy stress deviator $\boldsymbol{\sigma}'$ and the (Eulerian) viscoplastic strain-rate $\dot{\boldsymbol{\varepsilon}}_{vp}$. Under the rate-sensitivity approach to crystal plasticity, the constitutive behavior at each material point $\mathbf{x}$ belonging to a single crystal is described by means of the following non-linear relation between $\dot{\boldsymbol{\varepsilon}}_{vp}$ and $\boldsymbol{\sigma}'$:

$$\dot{\varepsilon}_{vp}(\mathbf{x}) = \sum_{k=1}^{N_k} m^k(\mathbf{x})\dot{\gamma}^k(\mathbf{x}) = \dot{\gamma}_o \sum_{k=1}^{N_k} m^k(\mathbf{x}) \left(\frac{|\mathbf{m}^k(\mathbf{x}) : \boldsymbol{\sigma}'(\mathbf{x})|}{\tau^k_o(\mathbf{x})} \right)^n \times \operatorname{sgn}\left(\mathbf{m}^k(\mathbf{x}) : \boldsymbol{\sigma}'(\mathbf{x})\right) \tag{14}$$

where the sum runs over all N_k slip and twinning systems. τ^k_o and $\mathbf{m}^k(\mathbf{x}) = \frac{1}{2}(\mathbf{n}^k(\mathbf{x}) \otimes \mathbf{b}^k(\mathbf{x}) + \mathbf{b}^k(\mathbf{x}) \otimes \mathbf{n}^k(\mathbf{x}))$ are, respectively, the threshold resolved shear stress and the symmetric Schmid tensor associated with slip or twinning system (k) (with $\mathbf{n}^k$ and $\mathbf{b}^k$ being the normal and Burgers vector direction of such slip or twinning system), $\dot{\gamma}^k$ is the local shear-rate on slip or twinning system (k), $\dot{\gamma}_o$ is a normalization factor and n is the rate-sensitivity exponent. Note that, in the case of twinning, the polarity of this mechanism can be taken into account, making τ^k_o a function of $\operatorname{sgn}(\mathbf{m}^k(\mathbf{x}) : \boldsymbol{\sigma}'(\mathbf{x}))$. The following linear relation (an approximation of the actual local non-linear relation, Eq. (14)) is assumed between $\dot{\boldsymbol{\varepsilon}}^{(r)}_{vp}$ and $\boldsymbol{\sigma}'^{(r)}$, i.e. the average

magnitudes of these fields inside each *mechanical phase* or *statistically-representative (SR) grain (r)*, representing the set of grains with the same orientation (r) and all possible neighborhoods compatible with the statistical description of the polycrystal:

$$\dot{\boldsymbol{\varepsilon}}^{(r)}_{vp} = \boldsymbol{M}^{(r)} : \boldsymbol{\sigma}'^{(r)} + \dot{\boldsymbol{\varepsilon}}^{o(r)} \tag{15}$$

where $\boldsymbol{M}^{(r)}$ and $\dot{\boldsymbol{\varepsilon}}^{o(r)}$ are respectively a linearized viscoplastic compliance and a back-extrapolated strain-rate of SR grain (r). Depending on the linearization assumption, $\boldsymbol{M}^{(r)}$ and $\dot{\boldsymbol{\varepsilon}}^{o(r)}$ can be chosen differently.[2] For instance, making use of the *affine* linearization (Masson et al., 2000):

$$\boldsymbol{M}^{(r)} = n\dot{\gamma}_o \sum_k \frac{\mathbf{m}^{k(r)} \otimes \mathbf{m}^{k(r)}}{\tau_o^{k(r)}} \left(\frac{\mathbf{m}^{k(r)} : \boldsymbol{\sigma}'^{(r)}}{\tau_o^{k(r)}} \right)^{n-1} \tag{16}$$

$$\dot{\varepsilon}^{o(r)} = (1-n)\dot{\gamma}_o \sum_k \left(\frac{\mathbf{m}^{k(r)} : \boldsymbol{\sigma}'^{(r)}}{\tau_o^{k(r)}} \right)^{n} \times \mathrm{sgn}(\mathbf{m}^{k(r)} : \boldsymbol{\sigma}'^{(r)}) \tag{17}$$

where the index (r) in $\mathbf{m}^{k(r)}$ and $\tau_o^{k(r)}$ indicates uniform (average) values of these magnitudes, corresponding to a given orientation and hardening state associated with SR grain (r).

The behavior of a linear heterogeneous medium, whose linear (piecewise constant) local response is described by Eq. (15), can be homogenized assuming an analogous linear relation at the effective medium (polycrystal, *px*) level:

$$\dot{\boldsymbol{\varepsilon}}^{(px)}_{vp} = \boldsymbol{M}^{(px)} : \boldsymbol{\sigma}'^{(px)} + \dot{\boldsymbol{\varepsilon}}^{o(px)} \tag{18}$$

where $\dot{\boldsymbol{\varepsilon}}^{(px)}_{vp}$ and $\boldsymbol{\sigma}'^{(px)}$ are the effective (polycrystal) deviatoric strain-rate and stress tensors and $\boldsymbol{M}^{(px)}$ and $\dot{\boldsymbol{\varepsilon}}^{o(px)}$ are respectively the *tangent viscoplastic compliance* and *back-extrapolated strain-rate* of an a priori unknown homogeneous medium that represents the behavior of the polycrystal. The usual procedure to obtain the homogenized response of a linear polycrystal is the linear self-consistent method. The problem underlying the self-consistent method is that of an inhomogeneous domain (r) of moduli $\boldsymbol{M}^{(r)}$ and $\dot{\boldsymbol{\varepsilon}}^{o(r)}$, embedded in an infinite medium of moduli $\boldsymbol{M}^{(px)}$ and $\dot{\boldsymbol{\varepsilon}}^{o(px)}$. Invoking the concept of the equivalent inclusion (Mura, 1987), Eqs. (15) and (18) can be combined to give:

$$\widetilde{\boldsymbol{\sigma}}'^{(r)} = \boldsymbol{L}^{(px)} : (\widetilde{\dot{\boldsymbol{\varepsilon}}}^{(r)}_{vp} - \dot{\boldsymbol{\varepsilon}}^{*(r)}) \tag{19}$$

where the symbol "$\sim$" denotes local deviations from macroscopic values of the corresponding magnitudes (e.g. $\widetilde{\boldsymbol{\sigma}}'^{(r)} = \boldsymbol{\sigma}'^{(r)} - \boldsymbol{\sigma}'^{(px)}$), $\boldsymbol{L}^{(px)} = [\boldsymbol{M}^{(px)}]^{-1}$ is the tangent viscoplastic stiffness, and $\dot{\boldsymbol{\varepsilon}}^{*(r)}$ is an eigen-strain-rate that fulfills Eshelby's relation:

$$\widetilde{\dot{\boldsymbol{\varepsilon}}}^{(r)}_{vp} = \boldsymbol{S} : \dot{\boldsymbol{\varepsilon}}^{*(r)} \tag{20}$$

where $\boldsymbol{S}$ is the (viscoplastic) symmetric Eshelby tensor, a function of $\boldsymbol{L}^{(px)}$ and the ellipsoidal shape that represents the morphology of the SR grains (for details of the calculation of $\boldsymbol{S}$, see Lebensohn et al. (2007)). Working with Eqs. (19) and (20), the following *interaction equation* is obtained:

$$\widetilde{\dot{\boldsymbol{\varepsilon}}}^{(r)}_{vp} = -\widetilde{\boldsymbol{M}} : \widetilde{\boldsymbol{\sigma}}'^{(r)} \tag{21}$$

where the interaction tensor is given by:

$$\widetilde{\boldsymbol{M}} = (\boldsymbol{I} - \boldsymbol{S})^{-1} : \boldsymbol{S} : \boldsymbol{M}^{(px)} \tag{22}$$

Replacing the constitutive relations of the inclusion and the effective medium in the interaction equation and after some manipulation one can write the following *localization equation*:

$$\boldsymbol{\sigma}'^{(r)} = \boldsymbol{B}^{(r)} : \boldsymbol{\sigma}'^{(px)} + \mathbf{b}^{(r)} \tag{23}$$

where the stress localization tensors are defined as:

$$\boldsymbol{B}^{(r)} = (\boldsymbol{M}^{(r)} + \widetilde{\boldsymbol{M}})^{-1} : (\boldsymbol{M}^{(px)} + \widetilde{\boldsymbol{M}}) \tag{24}$$

$$\mathbf{b}^{(r)} = (\boldsymbol{M}^{(r)} + \widetilde{\boldsymbol{M}})^{-1} : (\dot{\boldsymbol{\varepsilon}}^{o(px)} - \dot{\boldsymbol{\varepsilon}}^{o(r)}) \tag{25}$$

Replacing the stress localization equation (Eq. (23)) in the relation between average magnitudes of stress and strain-rate in (r) (Eq. (15)):

$$\boldsymbol{\varepsilon}^{(r)}_{vp} = \boldsymbol{M}^{(r)} : \boldsymbol{B}^{(r)} : \boldsymbol{\sigma}^{(px)} + \boldsymbol{M}^{(r)} : \mathbf{b}^{(r)} + \boldsymbol{\varepsilon}^{o(r)} \tag{26}$$

[2] Note that the VPSC code can run under different linearization assumptions, and that the corresponding results can differ substantially from each other when using the same hardening parameters. For a thorough discussion, see Lebensohn et al. (2007).

and taking volumetric average over the polycrystal while enforcing the condition that the average of the strain-rates over the aggregate has to coincide with the macroscopic quantities, i.e.:

$$\dot{\boldsymbol{\varepsilon}}_{vp}^{(px)} = \langle \dot{\boldsymbol{\varepsilon}}_{vp}^{(r)} \rangle \tag{27}$$

where the brackets "$\langle\rangle$" denote average over the SR grains, the following *self-consistent equations* for the polycrystal moduli are obtained:

$$\boldsymbol{M}^{(px)} = \langle \boldsymbol{M}^{(r)} : \boldsymbol{B}^{(r)} \rangle \tag{28}$$

$$\dot{\boldsymbol{\varepsilon}}^{o(px)} = \langle \boldsymbol{M}^{(r)} : \mathbf{b}^{(r)} + \dot{\boldsymbol{\varepsilon}}^{o(r)} \rangle \tag{29}$$

While the VPSC model can be interrogated with strain-rate imposed (i.e. $\dot{\boldsymbol{\varepsilon}}_{vp}^{(px)}$ fully applied and $\boldsymbol{\sigma}'^{(\mathbf{px})}$ to be determined); stress imposed (i.e. $\boldsymbol{\sigma}^{(px)}$ fully applied and $\dot{\boldsymbol{\varepsilon}}_{vp}^{(px)}$ to be determined); or mixed boundary conditions, the UMAT's algorithm has been conceived for stress-imposed boundary conditions. In such case, a typical VPSC calculation starts with a uniform stress initial guess: $\boldsymbol{\sigma}'^{(r)} = \boldsymbol{\sigma}'^{(px)}$, from where the corresponding initial guesses for $\dot{\boldsymbol{\varepsilon}}_{vp}^{(r)}$, $\boldsymbol{M}^{(r)}$ and $\dot{\boldsymbol{\varepsilon}}^{o(r)}$ can be readily obtained (Eqs. (14), (16), and (17)). Next, initial guesses for the polycrystal moduli are assumed (usually as simple averages of the local moduli). With them, and the applied stress, the initial guess for the polycrystal strain-rate can be obtained (Eq. (18)), and the Eshelby tensor can be computed, with the viscoplastic tangent stiffness and the ellipsoidal shape of the SR grains (for details, see Lebensohn et al. (2007)). Subsequently, the interaction tensor $\widetilde{\boldsymbol{M}}$ (Eq. (22)), and the localization tensors $\boldsymbol{B}^{(r)}$ and $\mathbf{b}^{(r)}$ (Eqs. (24) and (25)) can be calculated, as well. With these tensors, new estimates of $\boldsymbol{M}^{(px)}$ and $\dot{\boldsymbol{\varepsilon}}^{o(px)}$ are obtained by solving iteratively the self-consistent equations (Eqs. (28) and (29)). After achieving convergence on the macroscopic moduli (and, consequently, also on the macroscopic stress and the interaction and localization tensors), a new estimation of the average grain stresses can be obtained, using the localization relation (Eq. (23)). If the recalculated average grain stresses are different (within certain tolerance) from the input values, a new iteration is started, until convergence is reached. When the iterative procedure is completed, the average shear-rates on the slip system (k) in each SR grain (r) are calculated as:

$$\dot{\gamma}^{k(r)} = \dot{\gamma}_o \left(\frac{|\mathbf{m}^{k(r)} : \boldsymbol{\sigma}'^{(r)}|}{\tau_o^{k(r)}} \right)^n \times \mathrm{sgn}(\mathbf{m}^{k(r)} : \boldsymbol{\sigma}'^{(r)}) \tag{30}$$

These average shear-rates are in turn used to calculate the lattice rotation-rates associated with each SR grain, in *co-rotational axes*:

$$\dot{\boldsymbol{\omega}}^{(r)} = \widetilde{\dot{\boldsymbol{\omega}}}^{(r)} - \dot{\boldsymbol{\omega}}^{p(r)} \tag{31}$$

with:

$$\dot{\boldsymbol{\omega}}^{p(r)} = \sum_k \boldsymbol{\alpha}^{k(r)} \dot{\gamma}^{k(r)} \tag{32}$$

where $\boldsymbol{\alpha}^k(\mathbf{x}) = \frac{1}{2}(\mathbf{b}^k(\mathbf{x}) \otimes \mathbf{n}^k(\mathbf{x}) - \mathbf{n}^k(\mathbf{x}) \otimes \mathbf{b}^k(\mathbf{x}))$ is the antisymmetric Schmid tensor of system (k) in SR grain (r) and:

$$\widetilde{\dot{\boldsymbol{\omega}}}^{(r)} = \boldsymbol{\Pi} : \boldsymbol{S}^{-1} : \widetilde{\dot{\boldsymbol{\varepsilon}}}^{(r)} \tag{33}$$

with $\boldsymbol{\Pi}$ being the antisymmetric Eshelby tensor (Lebensohn et al., 2007).

The above numerical scheme can be used to predict the stress–strain response and the microstructure evolution of the polycrystal (crystallographic and morphologic texture and hardening evolution), by applying viscoplastic deformation to the polycrystal in incremental steps. The latter is done by assuming constant rates during a time interval Δt and using the strain-rates $\dot{\boldsymbol{\varepsilon}}_{vp}^{(r)}$ and rotation-rates $\dot{\boldsymbol{\omega}}^{(r)}$ (times Δt) to update the shape and orientation of the SR grains, and the shear-rates (times Δt) to update the critical stress of the deformation systems due to strain hardening, after each deformation increment. Concerning the evolution of the threshold stress with accumulated shear strain in each grain, an extended Voce law (Tomé et al., 1984) has been used, given by:

$$\tau^{*k(r)} = \tau_{oo}^k + (\tau_1^k + \theta_1^k \Gamma^{(r)})(1 - \exp(-\Gamma^{(r)} | \theta_o^k / \tau_1^k |)) \tag{34}$$

where $\Gamma^{(r)}$ is the total accumulated shear in the grain; τ_{oo}^k, τ_1^k, θ_o^k and θ_1^k are the initial threshold stress, the initial hardening-rate, the asymptotic hardening-rate and the back-extrapolated threshold stress, respectively. In addition, we allow for the possibility of "self" and "latent" hardening by defining coupling coefficients $h^{kk'}$, which empirically account for the obstacles that new dislocations (or twins) associated with system k' represent for the propagation of dislocations (or twins) on system k. The increase in the threshold stress is calculated as:

$$\Delta \tau_o^{k(r)} = \frac{d\tau^{*k(r)}}{d\Gamma^{(r)}} \sum_{k\prime} h^{kk'} \dot{\gamma}^{k'(r)} \Delta t \tag{35}$$

Note that the above (explicit) update scheme relies on the fact that the *internal variables* β_i that describe the microstructure (i.e. orientation, morphology and hardening state of each SR grain) evolve slowly within the adopted time interval. For later use, the increments can be compactly written as:

$$\Delta\boldsymbol{\varepsilon}_{vp}^{(px)} = \dot{\boldsymbol{\varepsilon}}_{vp}^{(px)}(\boldsymbol{\sigma}^{(px),t+\Delta t};\beta_i^t)\Delta t \tag{36}$$

$$\Delta\beta_i = \dot{\beta}_i(\boldsymbol{\sigma}^{(px),t+\Delta t};\beta_i^t)\Delta t \tag{37}$$

2.3. VPSC-based UMAT

While, for convenience, the elasto-viscoplastic algorithm to obtain the material response using the viscoplastic constitutive behavior provided by the polycrystal model will be hereby described in small-strain notation, this description is also applicable to finite deformations, replacing the small-strain variables by their analogous large-deformation ones, expressed in the co-rotational system (see Section 2.1). For large strains, it is necessary to save the actual orientation of each polycrystalline material point as an internal variable, e.g. to be able to represent the evolving texture in the fixed coordinate system (e.g. see Sections 3 and 4).

At macroscopic level, the applied load is divided in increments, and the equilibrium at each increment is obtained by means of the FE analysis in an iterative fashion, using a global non-linear solver. The load increment is controlled by the time, and once the problem has being solved at time t, the solution for the next time increment requires the polycrystal model to provide a tangent stiffness (Jacobian) matrix $\boldsymbol{C}^{tg} = \partial\Delta\boldsymbol{\sigma}/\partial\Delta\boldsymbol{\varepsilon}$ for each material point, in order for the FE scheme to compute an initial guess for the nodal displacements at $t + \Delta t$. The strain increments obtained from that prediction for each material point, $\Delta\boldsymbol{\varepsilon}^{FE}$, together with the stress $\boldsymbol{\sigma}^t$ and the set of internal state variables β_i^t corresponding to the previous increment, are used inside the UMAT to calculate a new guess for the stress and the Jacobian at $t + \Delta t$. When convergence in stress equilibrium is achieved by the global non-linear scheme, the new values (at $t + \Delta t$) of the stresses, the internal variables, and the Jacobian matrix are accepted for every node, and the calculation advances to the next increment. For a given $\Delta\boldsymbol{\varepsilon}^{FE}$, the VPSC-UMAT is based on the minimization of an ad-hoc residual, defined below.

The elastic constitutive relation for the stress in the material point at $t + \Delta t$ in the co-rotational system is given by:

$$\boldsymbol{\sigma}^{t+\Delta t} = \boldsymbol{\sigma}^t + \boldsymbol{C} : \Delta\boldsymbol{\varepsilon}_{el} = \boldsymbol{\sigma}^t + \boldsymbol{C} : (\Delta\boldsymbol{\varepsilon} - \Delta\boldsymbol{\varepsilon}_{vp}) \tag{38}$$

where $\boldsymbol{C}$ is the elastic stiffness of the polycrystal. In the present context, the natural choice for $\boldsymbol{C}$ is to use the elastic self-consistent (ELSC) estimate, given by (c.f. Eq. (28)):

$$\boldsymbol{C} = \langle \boldsymbol{C}^{(r)-1} : \boldsymbol{B}^{(r)} \rangle^{-1} \tag{39}$$

where $\boldsymbol{C}^{(r)}$ and $\boldsymbol{B}^{(r)}$ are the elastic stiffness and stress localization tensors (c.f. Eq. (24)) of SR grain (r). Note that an ELSC calculation for the determination of $\boldsymbol{C}$ is implemented in the VPSC code, at the beginning of each deformation increment. In this way, the textural changes are also accounted for in the determination of the polycrystalline material element's elastic modulus. Note also that the aforementioned choice amounts to effectively decouple the self-consistent determination of the elastic and viscoplastic response of the polycrystalline material points. This strategy, originally proposed by Mercier and Molinari (2009), obviously simplifies the determination of the polycrystal's constitutive behavior, although is less accurate than other, more involved, elasto-viscoplastic selfconsistent formulations recently proposed (e.g. Lahellec and Suquet, 2007a, 2007b; Doghri et al., 2010).

Combining Eq. (38) with the viscoplastic constitutive relation coming from VPSC (Eq. (36)), we obtain:

$$\Delta\boldsymbol{\varepsilon} = \boldsymbol{C}^{-1} : \Delta\boldsymbol{\sigma} + \Delta t\dot{\boldsymbol{\varepsilon}}_{vp}^{(px)}(\boldsymbol{\sigma}^t + \Delta\boldsymbol{\sigma};\beta_i^t) \tag{40}$$

We define a residual $\mathbf{X}(\Delta\boldsymbol{\sigma})$, as a (non-linear) function of the stress increment $\Delta\boldsymbol{\sigma} = \boldsymbol{\sigma}^{t+\Delta t} - \boldsymbol{\sigma}^t$, which the UMAT should return to the FE analysis, as the constitutive response of the polycrystalline material point to the trial strain increment $\Delta\boldsymbol{\varepsilon}^{FE}$:

$$\mathbf{X}(\Delta\boldsymbol{\sigma}) = \Delta\boldsymbol{\varepsilon} - \Delta\boldsymbol{\varepsilon}^{FE} = \boldsymbol{C}^{-1} : \Delta\boldsymbol{\sigma} + \Delta t\dot{\boldsymbol{\varepsilon}}_{vp}^{(px)}(\boldsymbol{\sigma}^t + \Delta\boldsymbol{\sigma};\beta_i^t) - \Delta\boldsymbol{\varepsilon}^{FE} \tag{41}$$

The condition $\mathbf{X}(\Delta\boldsymbol{\sigma}) = 0$ (i.e. $\Delta\boldsymbol{\varepsilon} = \Delta\boldsymbol{\varepsilon}^{FE}$), is obtained using a Newton–Raphson (NR) scheme to solve this non-linear algebraic equation. The corresponding Jacobian $\boldsymbol{J}_{NR}$ is given by:

$$\frac{\partial\mathbf{X}(\Delta\boldsymbol{\sigma})}{\partial(\Delta\boldsymbol{\sigma})} = \boldsymbol{J}_{NR}(\Delta\boldsymbol{\sigma}) = \boldsymbol{C}^{-1} + \Delta t\frac{\partial\dot{\boldsymbol{\varepsilon}}_{vp}^{(px)}}{\partial(\Delta\boldsymbol{\sigma})}(\boldsymbol{\sigma}^t + \Delta\boldsymbol{\sigma};\beta_i^t) = \boldsymbol{C}^{-1} + \Delta t\boldsymbol{M}^{(px)}(\boldsymbol{\sigma}^t + \Delta\boldsymbol{\sigma};\beta_i^t) \tag{42}$$

Hence, given a guess $\Delta\boldsymbol{\sigma}^{k-1}$ for the stress increment, the new guess is obtained as:

$$\Delta\boldsymbol{\sigma}^k = \Delta\boldsymbol{\sigma}^{k-1} - \boldsymbol{J}_{NR}^{-1}(\Delta\boldsymbol{\sigma}^{k-1}) : \mathbf{X}(\Delta\boldsymbol{\sigma}^{k-1}) \tag{43}$$

Moreover, using the first equalities of Eqs. (41) and (42):

$$\boldsymbol{J}_{NR} = \frac{\partial\mathbf{X}(\Delta\boldsymbol{\sigma})}{\partial(\Delta\boldsymbol{\sigma})} = \frac{\partial(\Delta\boldsymbol{\varepsilon} - \Delta\boldsymbol{\varepsilon}^{FE})}{\partial(\Delta\boldsymbol{\sigma})} = \frac{\partial(\Delta\boldsymbol{\varepsilon})}{\partial(\Delta\boldsymbol{\sigma})} \tag{44}$$

we obtain the Jacobian matrix that the VPSC-based UMAT should pass to the FE model:

$$\boldsymbol{C}^{tg} = \frac{\partial(\Delta\boldsymbol{\sigma})}{\partial(\Delta\boldsymbol{\varepsilon})} = \boldsymbol{J}_{NR}^{-1} = [\boldsymbol{C}^{-1} + \Delta t\boldsymbol{M}^{(px)}]^{-1} \tag{45}$$

Eq. (45) provides a closed expression for the FE Jacobian, as a function of the viscoplastic tangent moduli (which is calculated as part of the VPSC algorithm), the elastic stiffness of the aggregate, and the FE time increment. The use of this expression greatly reduces the overall computational cost because the polycrystal's stress and the elasto-viscoplastic tangent stiffness tensor are obtained from the same calculation loop. Moreover, the use of expression (45) for the FE Jacobian usually provides quadratic convergence to the macroscopic non-linear equations.

Finally, it must be remarked that the above procedure is semi-implicit: implicit in the stress value, because internal equilibrium is checked at the end of the increment, but explicit in the internal variables β_i (such as grain orientations, morphology and hardening variables). The reason for the proposed algorithm to remain explicit in those internal variables is related to the difficulty and computational cost of deriving a residual and a Jacobian matrix that would contain literally thousands of internal variables. In any case, the explicit updating of the internal variables appear not to change significantly the convergence of the macroscopic model in most cases, such that the influence of the time increment on the final results remains small, as it will be shown in the benchmark examples.

2.4. Finite element type

The proposed elasto-viscoplastic model was tested with several three-dimensional continuum elements. Linear cubic elements with reduced integration (C3D8R in ABAQUS) failed even for simple benchmarks due to the hourglass deformation modes. This behavior could not be corrected, even using an additional hourglass stiffness. All other typical solid elements (either linear or quadratic, hexahedra or tetrahedra) behaved adequately in this regard. Therefore, the choice of the type of element should be based on general aspects of the simulation of plastic deformation with finite elements, e.g. linear tetrahedra (C3D4 in ABAQUS) are not recommended since they exhibit volumetric locking, while hybrid formulations are specially suitable for large plastic deformations. Another important aspect to take into account for the choice of an element is that the main computational cost of the present FE implementation lies on the evaluation of constitutive behavior at the Gauss points by the relatively expensive VPSC model. Because of this, elements with the less integration points (compatible with non-hourglassing behavior) compared to the number of degrees of freedom are preferable. In this regard, quadratic elements with reduced integration were found to be a very good choice.

3. Benchmarks

In order to check the correct implementation and accuracy of the proposed multiscale model, we ran comparisons of the ABAQUS–VPSC model, against *stand-alone* (SA) VPSC calculations, for cases involving homogenous polycrystalline properties and simple boundary conditions, i.e. the type of configuration the stand-alone VPSC model can handle.

For this purpose, we used an FCC polycrystal represented by 500 initially randomly-oriented grains. The VPSC constitutive parameters, adjusted to reproduce the experimental behavior of an AA6116 Al alloy deformed in uniaxial compression (Tomé et al., 2002) were: τ_{oo} = 116 MPa, τ_1 = 119 MPa, θ_0 = 793 MPa and θ_1 = 31 MPa (see Eq. (34)), isotropic hardening ($h^{kk'} = 1, \forall kk'$, see Eq. (35)), and a rate-sensitivity exponent n = 10, in all 12 $\{1\,1\,1\}\langle 1\,1\,0\rangle$ slip systems. The single-crystal elastic constants used for Al were: C_{11} = 108 GPa, C_{12} = 62 GPa and C_{44} = 28 GPa.

The first benchmark corresponds to a uniaxial tensile test along the y-direction up to 50% strain. The FE model consisted in a single linear cubic element (8 nodes, and 8 integration points) with displacements imposed along the y-direction and stress-free boundary conditions on faces x–y and y–z. The applied strain-rate was $\dot{\varepsilon}_{yy} = 0.2$. In order to check the sensitivity of the predicted effective response to time-increment size, three different time increments were used, Δt = 0.05 s and 0.01 s (fixed), and adaptative time increments (i.e. the increment is reduced by half if no convergence is achieved) with a maximum step of 0.1 s and initial step of 0.01 s.

The stress–strain curves obtained with SA-VPSC and with ABAQUS–VPSC for the different time increments are presented in Fig. 1. One important difference between the FE and SA-VPSC predictions is that the latter is a rigid-viscoplastic model and obviously does not exhibit an elastoplastic transition. In what concerns the sensitivity of the macroscopic response to the magnitude of the time (strain) increment, it is observed that the FE predictions are insensitive to the time increment at sufficiently large strains and asymptotically tend to coincide with the SA-VPSC curve. On the other hand, time-step sensitivity appears to be significant in the elastoplastic transition, where the hardening rate varies rapidly. This sensitivity is due to the semi-implicit integration scheme, which becomes particularly inaccurate in this transition (note the initial non-smooth response predicted for the large (fixed) time step Δt = 0.05 s). These results suggest that for this initial part of the simulation smaller increments should be used. This can be achieved without much computational cost with an adaptative time increment, starting with small increments in the initial stage.

Concerning the rate of convergence of the material subroutine, in the case with largest strain increments, no more than 6 iterations were necessary inside the internal Newton–Raphson loop in the elastoplastic transition, and this number decreased to 2 iterations under fully plastic conditions. The convergence of the FE model was even better, with only 3 iterations needed in the initial increment in the worst case, and just one for the rest of the calculation. This result emphasizes the very efficient numerical behavior provided by the Jacobian matrix given by Eq. (45).

Another important check of our FE implementation, especially to verify that the intensive bookkeeping of internal variables is sound, is to compare the evolution of crystallographic orientations predicted by the FE model and the stand-alone

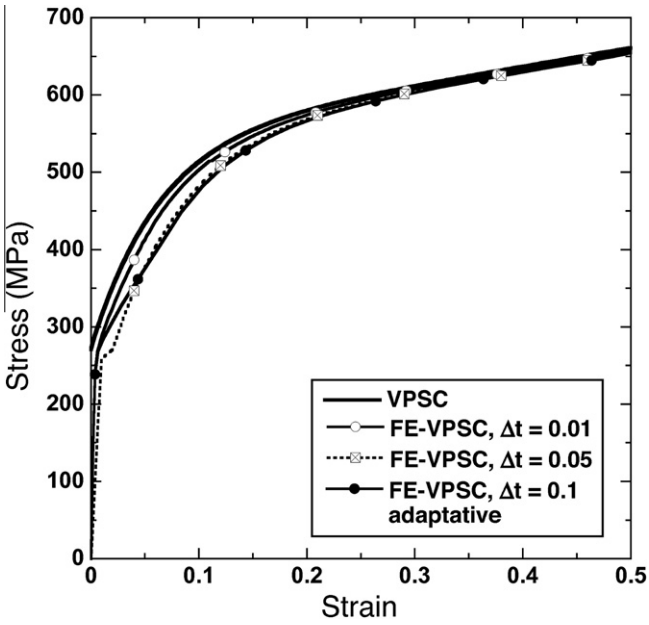

Fig. 1. Stress–strain curves for uniaxial tension of an FCC polycrystal obtained with SA-VPSC, and ABAQUS–VPSC using different time increments.

polycrystal model. Fig. 2 shows superimposed ⟨1 1 1⟩ pole figures predicted by SA-VPSC and ABAQUS–VPSC ($\Delta t = 0.01$ s). Instead of representing these uniaxial textures in the standard way (i.e. by means of inverse pole figures using level lines representing multiple of random distribution, which give compact and quantitative texture information), we use direct pole figures and plot one dot per pole per grain. In this way, we are able to show not only the good agreement between the overall textures predicted by our FE implementation and the reference SA-VPSC, but also the almost perfect match between the final orientations of individual grains predicted by both approaches, on a one-to-one basis.

Finally, a simple shear of the same FCC polycrystal was simulated with ABAQUS–VPSC and compared with the standalone case, for an applied deformation gradient $\mathbf{F} = \mathbf{I} + \gamma \mathbf{e}_y \otimes \mathbf{e}_z$, with $\gamma = 2$. This analysis was performed in order to check the correct treatment of rotations under finite-deformation kinematics. Fig. 3 shows the <111> pole figures corresponding to SA-VPSC (referred to the fixed initial axes, Fig. 3a), and ABAQUS–VPSC predictions in co-rotational axes (Fig. 3b), and ABA-

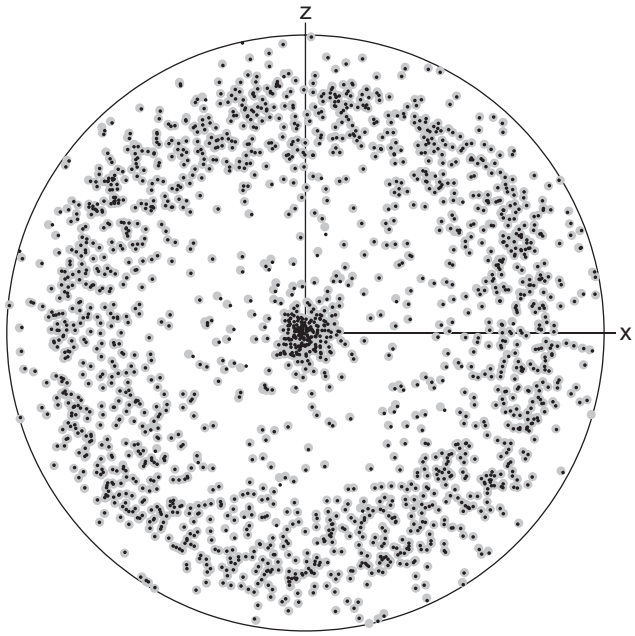

Fig. 2. Superimposed ⟨1 1 1⟩ direct pole figures predicted by SA-VPSC (larger gray dots) and ABAQUS–VPSC (smaller black dots) for 50% uniaxial tension of an FCC polycrystal.

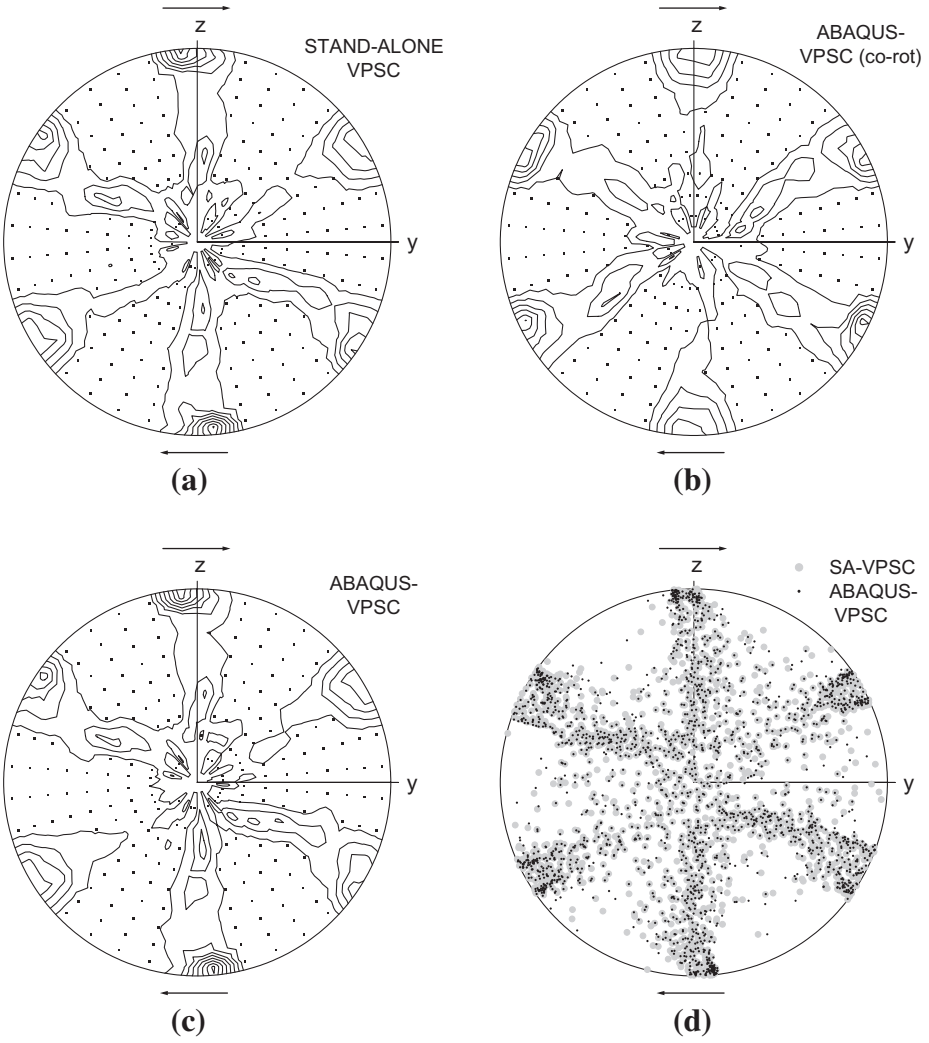

Fig. 3. ⟨1 1 1⟩ pole figures predicted by SA-VPSC and ABAQUS–VPSC for the case of simple shear ($\gamma_{yz} = 2$) of an FCC polycrystal. (a) SA-VPSC, in fixed axes; (b) ABAQUS–VPSC in co-rotational axes; (c) ABAQUS–VPSC in fixed axes. In all these figures, lines represent multiple of random distributions (mrd) and dots represent regions with less than 1 mrd. (d) SA-VPSC and ABAQUS–VPSC pole figures (in fixed axes) superimposed, using a one-dot-per-pole-per-grain representation.

QUS–VPSC in the same fixed reference system as the SA-VPSC texture (Fig. 3c). Note that both ABAQUS–VPSC pole figures are related by a rigid-body rotation of about 60 degrees defined by the rotation matrix **R** (see Section 2.1) that transforms from co-rotational to fixed axes. For this purpose the matrix **R** is stored by ABAQUS as another internal variable. The fact that the SA-VPSC and FE pole figures are almost identical when expressed in the same axes validates the proposed treatment of the crystallographic and rigid-body rotations. For a more detailed comparison, Fig. 3d shows the SA-VPSC and ABAQUS–VPSC pole figures superimposed, using a dot per pole per grain, instead of level lines. Again, the one-to-one matching of individual poles is very good, although somewhat larger differences can be appreciated for poles belonging to "outlier" grains (i.e. oriented differently with respect to the dominant shear texture components), whose final orientations seem to be more affected by the small differences in local mechanical behavior due to the consideration of elastic strains in the FE model (as opposed to the rigid-viscoplastic behavior under SA-VPSC).

4. Applications

4.1. Texture variations in a rolled FCC plate

To further illustrate the capabilities of the proposed multiscale model, a rolling process of the same FCC material (AA6016 Al-alloy) has been simulated to capture the spatial variations of texture evolution. These variations, in turn, change the local

behavior and, as a consequence, determine the redistribution of stresses during deformation. This case constitutes a challenge for the proposed approach, since it includes heterogeneous deformation, large strains and rotations, contact and complex local strain histories, including unloading at the exit (which cannot be handled by a rigid-viscoplastic model).

The simulation consists of a single rolling pass of 50% reduction in thickness (from 1 to 0.5, in arbitrary length units). Plane-strain is imposed (no strain in the transverse direction, TD, aligned with the z-axis), and symmetry is used to reduce the size of the FE model. Load is applied by the rotation of two rolling cylinders of radius $R = 4$. An initial step consists in a small vertical displacement of the cylinders in order to establish contact conditions between rolls and plate at the entry and, subsequently, rotation with an angular velocity $\omega = 2\ s^{-1}$ until the plate has been completely rolled.

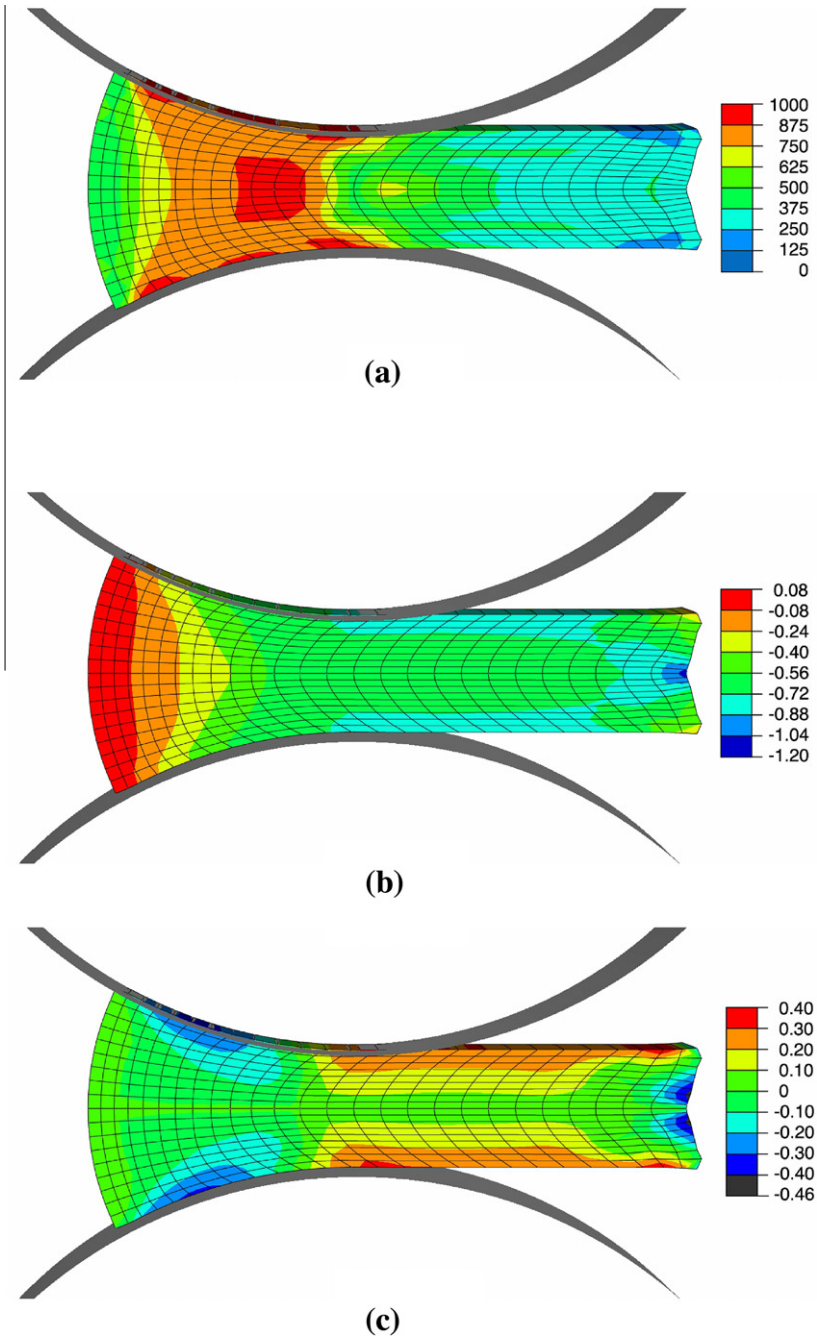

Fig. 4. ABAQUS–VPSC simulation of rolling of an FCC plate, up to 50% reduction. Distributions of: (a) Von Mises stress (in MPa), (b) diagonal strain component in ND and (c) shear strain component along RD normal to ND.

The movement of the cylinders is transferred to the plate by friction, and the imposed angular velocity corresponds to an average compression strain-rate component of 2.1 s^{-1} along the normal direction (ND, y-axis). The plate of initial size 4×1 in the rolling (RD, x-axis)-ND plane, is meshed with a structured mesh of linear cubes with full integration (C3D8 in ABAQUS) using 26×9 elements in that plane and 1 element in TD. The geometry in the final stage is shown in Fig. 4, together with the corresponding distributions of Von Mises stress, the diagonal strain component in ND, ε_{yy}, and the shear strain ε_{xy}. Interestingly, the stress does not vanish in the region already laminated and a heterogeneous distribution of residual stresses is left in the material. Both from Fig. 4c and the final shape of the elements it can be concluded that elements near the surface underwent significant shear deformation along RD normal to ND, while elements towards the center were subjected to smaller shear distortion. This shear deformation is a consequence of the friction between the metal surface and the cylinders.

The different deformation history of the polycrystalline material points through the section determines different evolution of the texture. In order to study this effect, the texture has been tracked in two material points, located near the center and near the surface of the plate, respectively. Both points were taken far from the leading tip in the rolling direction in order to minimize edge effects and obtain results that resemble those of a continuum rolling process. The $\langle 1\,1\,1 \rangle$ pole figures of both polycrystalline material points are shown in Fig. 5. It is observed that the textures near the center resemble typical plane-strain compression textures of high-SFE FCC polycrystals, while the texture associated with a point near the surface shows significant rotation with respect to TD of the rolling texture components, consistent with a plane-strain + shear strain history applied to the material point. Similar results were reported by Engler et al. (2000), in terms of experimental Al rolling textures and SA-VPSC texture predictions using FE-generated deformation histories.

4.2. Dimensional changes in bent HCP bars

Four-point bending experiments performed on textured Zr (Tomé et al., 2001; Kaschner et al., 2001) and Ti (Nixon et al., 2010a) bars have been used to illustrate the strong effect of texture-induced anisotropy on the mechanical response of HCP polycrystals. These experiments consisted in the bending of bars of square cross-section, cut from the same plate, with their main basal texture component oriented either perpendicular or parallel to the bending plane. This geometry resulted in different dimensional changes of the cross-sections of the bars, which can be explained in terms of texture-related "hard" or "soft" responses normal to the fibers along the longitudinal direction. These fibers undergo tension or compression, depending on its vertical position.

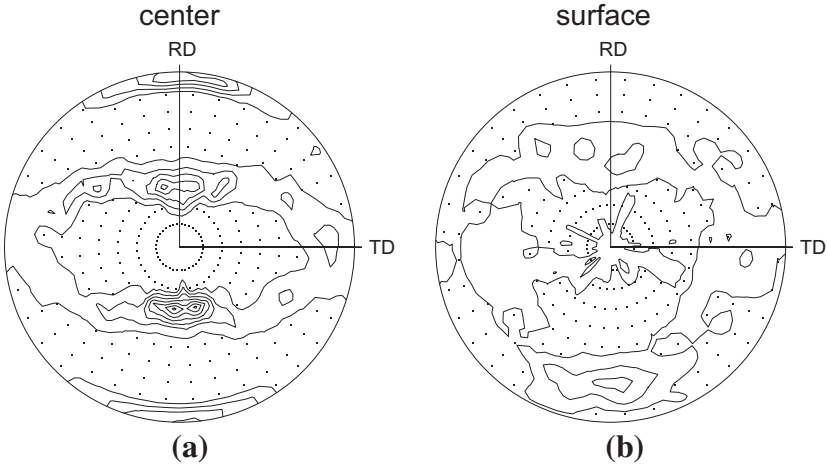

Fig. 5. $\langle 1\,1\,1 \rangle$ pole figures predicted by ABAQUS–VPSC in the case of rolling of an FCC plate after 50% reduction, for two polycrystalline material points located: (a) near the center, and (b) near the surface of the plate. Lines represent multiple of random distributions (mrd) and dots represent regions with less than 1 mrd.

Table 1
VPSC parameters used in the VPSC–ABAQUS simulations of 4-point bending of textured Zr bars (from Tomé and Lebensohn, 2011).

	τ_0 (MPa)	τ_1 (MPa)	θ_0 (MPa)	θ_1 (MPa)	$h^{*,PR}$	$h^{*,PY}$	$h^{*,TT}$	$h^{*,CT}$	n
Pr$\langle a \rangle$	14	12	900	40	1	1	10	2	10
Pyr$\langle c + a \rangle$	145	192	1684	5	1	1	2	2	10
TT1	90	17	100	30	1	1	10	16	10
CT1	270	30	1000	178	1	1	10	5	10

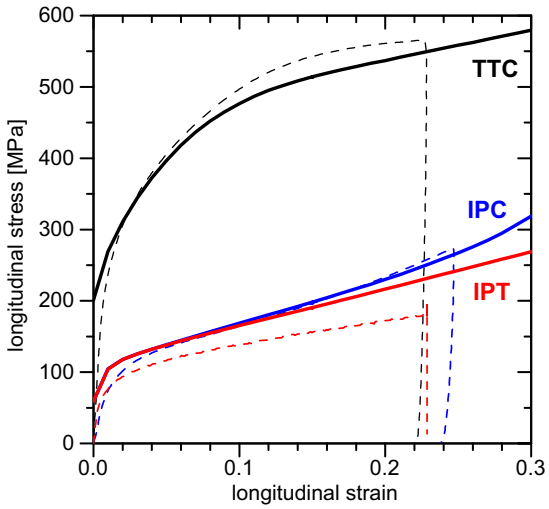

Fig. 6. Measured (after Tomé et al., 2001) and VPSC stress–strain curves (after Tomé and Lebensohn, 2011) corresponding to three different uniaxial tests performed on the textured Zr plate from where bars for 4-point bending experiments were cut.

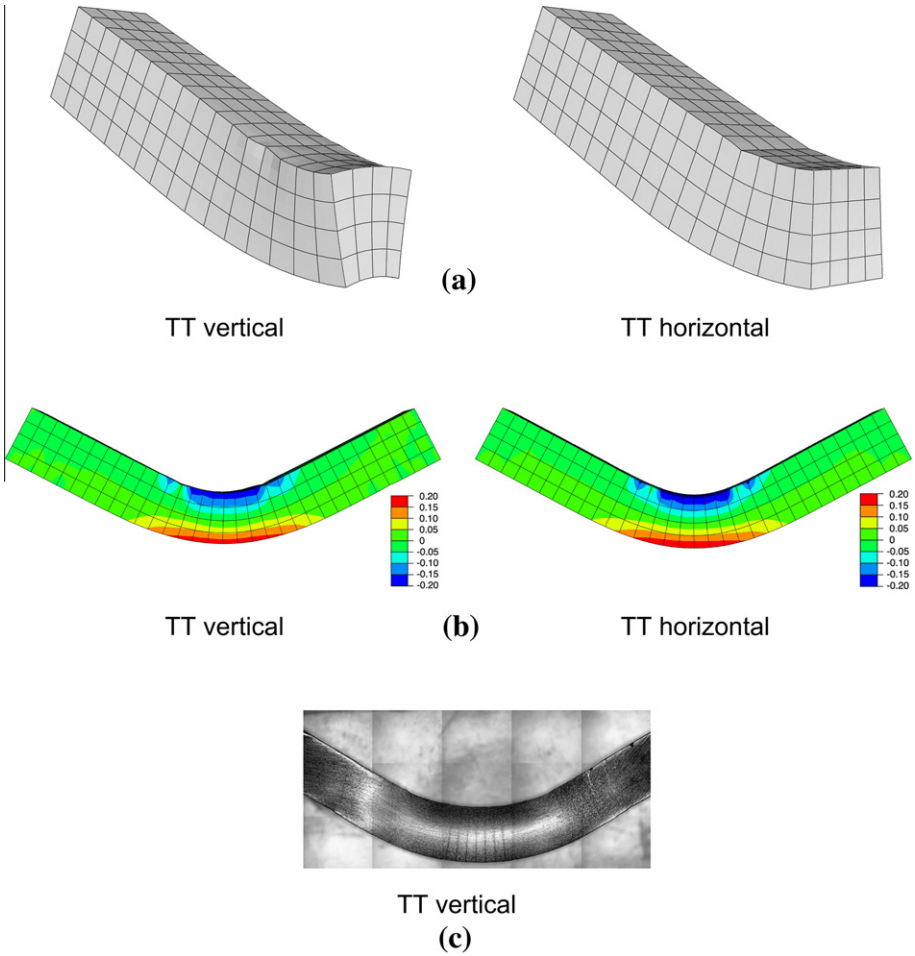

Fig. 7. Four-point bending of textured Zr bars, up to approximately 20% strain in the outer fibers. (a) Predicted final 3-D shapes, (b) predicted final lateral sections, showing the distribution of strain component along the fiber direction; (c) montage of the actual deformed sample (TT vertical), from Kaschner et al. (2001).

These experiments were in turn modeled with texture-sensitive explicit finite elements, using both a hierarchical approach (see Plunkett et al. (2006) for Zr, and Nixon et al. (2010b) for Ti), in which the FE analysis interrogated a pre-computed anisotropic yield function whose parameters were adjusted using experimental data (Plunkett et al., 2006; Nixon et al., 2010b, supplemented by VPSC simulations in Plunkett et al., 2006), and also using a fully-embedded approach (Tomé et al., 2001; Kaschner et al., 2001). Here we will use the proposed VPSC–ABAQUS implementation to reproduce the 4-point bending experiments in Zr (Tomé et al., 2001; Kaschner et al., 2001). The initial axisymmetric texture of the bars (i.e. transversely-isotropic in the plane of the plate from where the bars were cut) is represented by 377 orientations with basal poles predominantly aligned with the normal direction of the original plate (Tomé et al., 2001; Tomé and Lebensohn, 2011). The slip and twinning modes used in the simulations were those identified by Tomé et al. (2001): $\{1\,0\,\bar{1}\,0\}\langle\bar{1}\,2\,\bar{1}\,0\rangle$ prismatic $\langle a\rangle$ slip (Pr$\langle a\rangle$), $\{1\,0\,\bar{1}\,1\}\langle\bar{1}\,\bar{1}\,2\,3\rangle$ pyramidal $\langle c+a\rangle$ slip (Pyr$\langle c+a\rangle$), $\{1\,0\,\bar{1}\,2\}\langle1\,0\,\bar{1}\,\bar{1}\rangle$ tensile twinning (TT1) and $\{1\,1\,\bar{2}\,2\}\langle1\,1\,\bar{2}\,\bar{3}\rangle$ compressive twinning (CT1). The corresponding hardening parameters, given in Table 1, were adjusted (Tomé and Lebensohn, 2011) to reproduce to the best extent possible loading curves of uniaxial in-plane tension (IPT), uniaxial in-plane compression (IPC) and through-thickness compression (TTC) experiments, performed at a strain-rate of $10^{-3}\,s^{-1}$, as shown in Fig. 6. Note these hardening parameters have differences with respect to the ones used in Tomé et al. (2001). Such adjustment was required to better approach the experimental curves using the latest version of VPSC (Tomé and Lebensohn, 2011), which includes, e.g. an improved integration-based update for the hardening of individual systems. Reorientation by twinning was handled within VPSC by means of the "Predominant Twin Reorientation" (PTR) scheme, originally proposed by Tomé et al. (1991), and also used in Tomé et al. (2001), which allows keeping track of the textural changes associated with twinning in a statistical sense, without increasing the number of orientations needed for the representation of each polycrystalline materials point (for details, see Tomé et al. (1991, 2001)). Note that all quantities associated with the PTR scheme were required to be defined as additional internal variables within the UMAT.

The bars of initial dimensions $6.35 \times 6.35 \times 50.8$ mm were discretized using a structured mesh of $32 \times 4 \times 4$ quadratic elements (20 nodes with reduces integration, C3D20R). Two external steel pins, fixed underneath the bar, and two internal pins, moving downwards from the top, all of them of 6.32 mm diameter, were set at center-to-center distances of ±19.05 mm and ±6.35 mm, respectively. The total displacement of the upper pins was −6 mm, corresponding to a longitudinal strain of the most external fiber of approximately +20%.

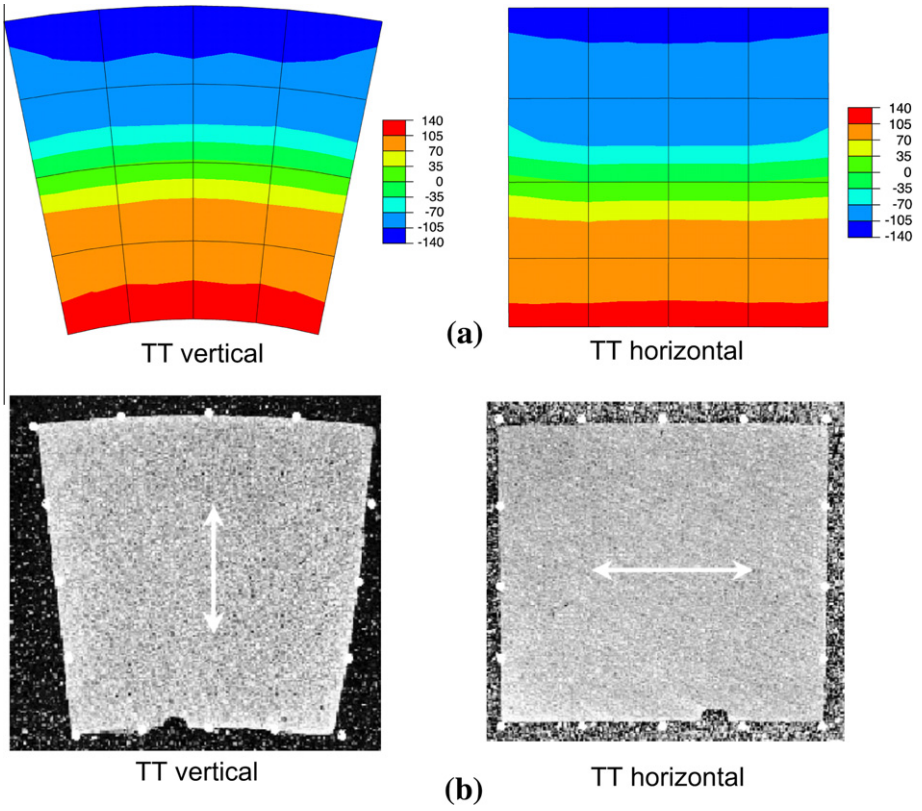

Fig. 8. Four-point bending of textured Zr bars. (a) Predicted final cross-sections, showing the distribution of the stress component along the fiber direction (in MPa); (b) measured cross-sections (Kaschner et al., 2001), white arrows represent the predominant direction of the basal poles.

In order to reproduce previously reported experiments (Tomé et al., 2001; Kaschner et al., 2001), two different geometries, in terms of the predominant orientation of the basal poles (aligned with the TT direction of the original plate) with respect to the bending plane were simulated, for bars cut along the IP direction of the plate. In one case, the hard TT direction lies on the bending plane (i.e. *TT vertical*), while in the other configuration, the TT direction is perpendicular to the bending plane (i.e. *TT horizontal*). Fig. 7 shows the predicted 3-D final shapes, together with the lateral views (with color[3] maps representing the strain component along the fiber direction), and a montage of the actual deformed sample in the *TT vertical* case, reported by Kaschner et al. (2001). While the lateral views show little differences (both in terms of final shape and accumulated longitudinal strain) and resemble the experimental image, the 3-D views of the deformed bars show the strong effect that texture had on the final shape. Because in the *TT horizontal* case the horizontal direction on the bar cross section is hard to deform, the lateral section remains almost flat, in contrast with the *TT vertical* case, in which the lateral section becomes strongly warped. These strong differences between both bar orientations can also be observed in Fig. 8, which shows the cross sections of the bars (color maps correspond to the longitudinal stress component), together with the actual measured shapes (Kaschner et al., 2001), with the white arrows representing the predominant direction of the basal poles. It is evident that when the texture-induced soft (respectively, hard) direction of the polycrystalline Zr bar lies horizontally, a strongly wedged (respectively, almost square) cross-section is predicted, in good agreement with the experimental observations. Note that these striking differences in the cross-section's strains have little influence on the stress component along the fiber direction, which in both cases remains aligned with the soft IP direction of the original plate. Only FE models using texture-sensitive constitutive responses (provided in this case by the VPSC model) are capable to capture these effects. Finally, it is also worth comparing the efficiency of the present implicit implementation and the explicit one of Tomé et al. (2001) applied to the same problem. While Tomé et al.'s explicit calculation required 16,000 time steps, the present implicit simulation was completed after only 45 time increments.

5. Conclusions

A multiscale FE model for the prediction of plastic deformation of polycrystalline materials, in which each integration point is in itself a polycrystal with evolving texture, has been developed and embedded in ABAQUS-implicit. The VPSC code (Lebensohn and Tomé, 1993; Tomé and Lebensohn, 2011) is used to localize the macroscopic fields in the single crystals whose distribution represents the texture associated with each material point, and to provide the homogenized viscoplastic response of these FE nodes. The integration of the non-linear material equations is semi-implicit and the convergence is fast, both at mesoscopic (polycrystal) and macroscopic levels. The key for this fast convergence is the use of Eq. (45), which gives the FE elasto-viscoplastic Jacobian as a function of elastic and viscoplastic self-consistent moduli, already calculated inside VPSC as part of the polycrystal model solution. However, despite this efficient algorithm, it should be acknowledged that the intensive use of VPSC evaluations, along with the required bookkeeping of thousands of internal variables associated with the orientation and hardening state of each grain in each polycrystalline integration point, add significantly to the computing time and memory requirements of the proposed FE approach.

Simple geometries and boundary conditions, corresponding to uniaxial tension and simple shear of a single element, were solved using the proposed ABAQUS–VPSC and compared with stand-alone VPSC predictions. These comparisons showed that, past the elastoplastic transition, the macroscopic behavior predicted by the FE model was very similar to the reference SA-VPSC. The FE response is mildly dependent on the magnitude of the time/strain increment, mostly in the elastoplastic transition, and is almost completely independent of the increment size for large plastic deformations. In what concerns texture evolution, the ABAQUS–VPSC predictions match very well those of SA-VPSC, on a grain-by-grain basis. This is specially significant in the case of simple shear, i.e. involving large rotations, which therefore serves as validation of the underlying kinematics of our implementation.

In terms of applications, two illustrative examples were shown in the cases of rolling of FCC and bending of HCP polycrystals. In the first case, the use of the FE model allowed us to keep track of the effect of the macro-strain heterogeneity (induced by the complex boundary conditions) on the texture evolution at different locations of a mechanically-processed material. The different evolving elastic and viscoplastic responses of the FE polycrystalline points associated with those texture gradients in turn affect the overall mechanical behavior of the deformed specimen. This texture-sensitive response is critical to improve predictions of, e.g., industrial forming operations, in which textural effects are known to play a significant role on the dimensions, shape, spring-back and mechanical state (e.g. residual stresses) of the final product. The present coupling between these well-established formulations, VPSC and ABAQUS, provides a useful numerical tool to tackle these problems. In this regard, the second application shown above, corresponding to the prediction of dimensional changes associated with different orientations of the predominant texture component of an HCP bar undergoing 4-point bending, exemplifies the capability now in place with ABAQUS–VPSC to account for texture-induced effects in strongly anisotropic materials undergoing complex boundary conditions.

Finally, it should be emphasized that, while in the above applications a relatively standard version of the VPSC model was used (e.g. Voce hardening, first-order linearizations), other more involved approaches, already implemented in VPSC to capture more of the underlying physics and microstructural effects, can be easily adapted to provide a more sophisticated

[3] For interpretation of color in Figs. 7 and 8, the reader is referred to the web version of this article.

microstructure-sensitive material response under ABAQUS. These VPSC extensions include the *composite-grain model* (Proust et al., 2007), designed to capture the strongly anisotropic slip-twin interactions and the use of dislocation-density based hardening models (Beyerlein and Tomé, 2008), which includes grain-size and kinematic hardening effects, along with more accurate linearization assumptions, like the *second-order* self-consistent approximation (Liu and Ponte Castaneda, 2004), which has been shown to improve the VPSC predictions for strongly anisotropic materials (Lebensohn et al., 2007) and voided polycrystals (Lebensohn et al., 2011).

Acknowledgments

The authors wish to thank Nathan Barton (LLNL) for fruitful discussions. J.S. and J.LL. acknowledge support from Ministry of Science and Innovation of Spain, Grant MAT2009-14396, and by Comunidad de Madrid, ESTRUMAT program (S2009/MAT-1585). R.A.L.'s work supported by US Department of Energy under contract DE-AC52-06NA25396. C.N.T. acknowledges support from the US Department of Energy, Office of Basic Energy Sciences, project FWP-06SCPE401.

References

ABAQUS, 2007. User's Manual, v.6.7.
Asaro, R.J., Needleman, A., 1985. Texture development and strain hardening in rate dependent polycrystals. Acta Metallurgica 33, 923–953.
Barton, N.R., Knap, J., Arsenlis, A., Becker, R., Hornung, R.D., Jefferson, D.R., 2008. Embedded polycrystal plasticity and adaptive sampling. International Journal of Plasticity 24, 242–266.
Beyerlein, I.J., Tomé, C.N., 2007. Modeling transients in the mechanical response of copper due to strain path changes. International Journal of Plasticity 23, 640–664.
Beyerlein, I.J., Tomé, C.N., 2008. A dislocation-based constitutive law for pure Zr including temperature effects. International Journal of Plasticity 24, 867–895.
Delannay, L., Jacques, P.J., Kalidindi, S.R., 2006. Finite element modeling of crystal plasticity with grains shaped as truncated octahedrons. International Journal of Plasticity 22, 1879–1898.
Doghri, I., Adam, L., Bilger, N., 2010. Mean-field homogenization of elasto-viscoplastic composites based on a general incrementally affine linearization method. International Journal of Plasticity 26, 219–238.
Engler, O., Huh, M.Y., Tomé, C.N., 2000. A study of through-thickness texture gradients in rolled sheets. Metallurgical and Materials Transactions 31A, 2299–2315.
Feyel, F., 2003. A multilevel finite element method (FE2) to describe the response of highly non-linear structures using generalized continua. Computational Methods in Applied Mechanics and Engineering 192, 3233–3244.
Hershley, A.V., 1954. The elasticity of an isotropic aggregate of anisotropic cubic crystals. Journal of Applied Mechanics 21, 236–240.
Kalidindi, S.R., 1998. Incorporation of deformation twinning in crystal plasticity models. Journal of the Mechanics and Physics of Solids 46, 269–290.
Kalidindi, S.R., Bronkhorst, C.A., Anand, L., 1992. Crystallographic texture evolution in bulk deformation processing of fcc metals. Journal of the Mechanics and Physics of Solids 40, 537–569.
Kaschner, G.C., Bingert, J.F., Liu, C., Lovato, M.L., Maudlin, P.J., Stout, M.G., Tomé, C.N., 2001. Mechanical response of zirconium: II. Experimental and finite element analysis of bent beams. Acta Materialia 49, 3097–3108.
Kouznetsova, V.G., Geers, M.G.D., 2008. A multi-scale model of martensitic transformation plasticity. Mechanics of Materials 40, 641–657.
Lahellec, N., Suquet, P., 2007a. On the effective behavior of nonlinear inelastic composites. I. Incremental variational principles. Journal of the Mechanics and Physics of Solids 55, 1932–1965.
Lahellec, N., Suquet, P., 2007b. the effective behavior of nonlinear inelastic composites. II. A second-order procedure. Journal of the Mechanics and Physics of Solids 55, 1964–1992.
Lebensohn, R.A., Tomé, C.N., 1993. A selfconsistent approach for the simulation of plastic deformation and texture development of polycrystals: application to Zirconium alloys. Acta Metallurgica et Materialia 41, 2611–2624.
Lebensohn, R.A., Tomé, C.N., Ponte Castañeda, P., 2007. Self-consistent modeling of the mechanical behavior of viscoplastic polycrystals incorporating intragranular field fluctuations. Philosophical Magazine 87, 4287–4322.
Lebensohn, R.A., Idiart, M.I., Ponte Castañeda, P., Vincent, P.G., 2011. Dilatational viscoplasticity of polycrystalline solids with intergranular cavities. Philosophical Magazine 91, 3038–3067.
Liu, Y., Ponte Castaneda, P., 2004. Second-order theory for the effective behavior and field fluctuations in viscoplastic polycrystals. Journal of the Mechanics and Physics of Solids 52, 467–495.
Masson, R., Bornert, M., Suquet, P., Zaoui, A., 2000. Affine formulation for the prediction of the effective properties of nonlinear composites and polycrystals. Journal of the Mechanics and Physics of Solids 48, 1203–1227.
Mathur, K.K., Dawson, P.R., 1989. On modeling the development of crystallographic texture in bulk forming processes. International Journal of Plasticity 5, 67–94.
Miehe, C., Schroeder, J., Schotte, J., 1999. Computational homogenization analysis in finite plasticity, simulation of texture development in polycrystalline materials. Computational Methods in Applied Mechanics and Engineering 171, 387–418.
Mercier, S., Molinari, A., 2009. Homogenization of elastic-viscoplastic heterogeneous materials: self-consistent and Mori–Tanaka schemes. International Journal of Plasticity 25, 1024–1048.
Molinari, A., Canova, G.R., Ahzi, S., 1987. Self-consistent approach of the large deformation polycrystal viscoplasticity. Acta Metallurgica 35, 2983–2994.
Mura, T., 1987. Micromechanics of Defects in Solids. Martinus-Nijhoff Publishers, Dordrecht.
Nixon, M.E., Cazacu, O., Lebensohn, R.A., 2010a. Anisotropic response of high-purity alpha-titanium. Experimental characterization and constitutive modelling. International Journal of Plasticity 26, 516–532.
Nixon, M.E., Lebensohn, R.A., Cazacu, O., Liu, C., 2010b. Experimental and finite-element analysis of the anisotropic response of high-purity alpha-titanium in bending. Acta Materialia 58, 5759–5767.
Peeters, B., Hoferlin, E., Van Houtte, P., Aernoudt, E., 2001. Assessment of crystal plasticity calculation of lattice spin of polycrystalline metals for FE implementation. International Journal of Plasticity 17, 819–836.
Peirce, D., Asaro, R.J., Needleman, A., 1982. An analysis of nonuniform and localized deformation in ductile single crystals. Acta Metallurgica 30, 1087–1119.
Plunkett, B., Lebensohn, R.A., Cazacu, O., Barlat, F., 2006. Evolving yield function of hexagonal materials taking into account texture development and anisotropic hardening. Acta Materialia 54, 4159–4169.
Proust, G., Tomé, C.N., Kaschner, G.C., 2007. Modeling texture, twinning and hardening evolution during deformation of hexagonal materials. Acta Materialia 55, 2137–2148.
Roters, F., Eisenlohr, P., Hantcherli, L., Tjahjanto, D.D., Bieler, T.R., Raabe, D., 2010. Overview of constitutive laws, kinematics, homogenization and multiscale methods in crystal plasticity finite-element modeling: theory, experiments, applications. Acta Materialia 58, 1152–1211.

Tomé, C., Canova, G.R., Kocks, U.F., Christodoulou, N., Jonas, J.J., 1984. The relation between macroscopic and microscopic strain-hardening in fcc polycrystals. Acta Metallurgica 32, 1637–1653.
Tomé, C.N., Lebensohn, R.A., Kocks, U.F., 1991. A model for texture development dominated by deformation twinning: application to Zirconium alloys. Acta Metallurgica et Materialia 39, 2667–2680.
Tomé, C.N., Maudlin, P.J., Lebensohn, R.A., Kaschner, G.C., 2001. Mechanical response of zirconium: I. Derivation of a polycrystal constitutive law and finite element analysis. Acta Materialia 49, 3085–3096.
Tomé, C.N., Lebensohn, R.A., Necker, C.T., 2002. Orientation correlations and anisotropy of recrystallized aluminum. Metallurgical and Materials Transactions 33A, 2635–2648.
Tomé C.N., Lebensohn R.A., 2011. Manual for Code Viscoplastic Self-consistent (version 7c). <http://public.lanl.gov/lebenso/vpsc7c_manual.pdf>.
Van Houtte, P., Kanjarla, A.K., Van Bael, A., Seefeldt, M., Delannay, L., 2006. Multiscale modelling of the plastic anisotropy and deformation texture of polycrystalline materials. European Journal of Mechanics A/Solids 25, 634–648.
Van Houtte, P., Yerra, S.K., Van Bael, A., 2009. The Facet method: a hierarchical multilevel modelling scheme for anisotropic convex plastic potentials. International Journal of Plasticity 25, 332–360.
Walde, T., Riedel, H., 2007a. Simulation of earing during deep drawing of magnesium alloy AZ31. Acta Materialia 55, 867–874.
Walde, T., Riedel, H., 2007b. Modeling texture evolution during hot rolling of magnesium alloy AZ31. Materials Science and Engineering A 443, 277–284.
Werwer, M., Cornec, A., 2000. Numerical simulation of plastic deformation and fracture in polysynthetically twinned (PST) crystals of TiAl. Computational Materials Science 19, 97–107.